(Received 17 November 2024, Accepted 3 January 2025, Scheduled 18 January 2025)

A Miniaturized Quad Port Highly Isolated Triple Band Notched UWB-MIMO Diversity Antenna

Thotakura Sushma[1], Rajesh Gogineni[2], Nallagonda Vijaya Ratnam[2], Sadineni Ramesh Babu[3,*], Sunitha Mandava[3], and Paruchuri V. Krishna Kanth[3]

[1]*Department of Electronics & Communication Engineering, PVP Siddhartha Institute of Technology, Vijayawada, India*
[2]*Department of Electronics & Communication Engineering, Dhanekula Institute of Engineering and Technology, Ganguru, India*
[3]*Department of Electronics & Communication Engineering, RVR & JC College of Engineering, Guntur 522019, India*

ABSTRACT: In this study, a quad-port ultra-wideband (UWB) multiple input multiple output (MIMO) antenna with triple band-rejection characteristics is demonstrated. The suggested diversity MIMO antenna comprises four similar rectangular radiators positioned in orthogonal manner by utilizing polarization diversity. For superior inter-element isolation, a fan-shaped decoupler is lithographed on the back of the substrate. The MIMO antenna exhibits an operational bandwidth of 9 GHz (3–12 GHz) for each port, with $|S_{11}| \leq -10$ dB. This version is more concise and properly formatted. The MIMO aerial exhibits an impedance bandwidth 3–12 GHz) for each port ($|S_{11}| \leq -10$ dB) along with an inter-element isolation exceeding 20 dB. Additionally, to exclude the 3.5–4.1 GHz (downlink C-band), 4.43–4.79 GHz (INSAT), and 5.25–5.71 GHz (Wireless LAN) bands that coexist in UWB spectrum, the antenna elements are equipped with three U-shaped slots. The MIMO diversity metrics, including isolation, envelope correlation coefficient, diversity gain, TARC, CCL, multiplexing efficiency, and group delay, were computed and reported. The reported aerial prototype has been constructed, and the measured results have been validated against the simulated findings.

1. INTRODUCTION

In 2002, the Federal Communications Commission (FCC) empowered the usage of ultra-wideband (UWB) bandwidth (3.1–10.6 GHz) meant for data communication [1]. However, UWB antennas are susceptible to multipath fading [2]. The utilization of UWB alongside multiple-input multiple-output (MIMO) antenna technology enhances transmission capacity and reliability while also reducing multi-path fading [3]. MIMO improves reliability by using multiple antennas at both the transmitter and receiver. Mutual coupling predominates with the existence of many antennas. A variety of techniques, such as neutralization lines [4], parasitic elements [5], defected ground structure (DGS) [6], have been proposed to mitigate intrusion across aerials. The principal issue in the design of UWB aerials was the risk of intrusion from narrowbands, stemming with the necessity to share frequencies. Numerous narrowband technologies, including Worldwide Interoperability for Microwave Access (3.1–3.9 GHz), C-band (3.7–4.2 GHz), Indian National Satellite System (4.3–4.9 GHz), Wireless LAN (5.1–5.9 GHz), and X-band (7.7–8.4 GHz), are present in UWB. Implementing frequency rejection filters at the output of the aerial is an effective method for eliminating certain frequencies. Nonetheless, it will augment the complexity of the aerial. Consequently, attaining rejection qualities while minimizing implementation complexity is challenging. To reduce interference from different frequencies, an antenna designed to reject signals from multiple frequencies is used. Numerous researchers have proposed diverse methods for designing antennas capable of attenuating signals throughout one, dual, or triple frequencies. A MIMO aerial including twin quasi-self-complementary antennas are engineered to mitigate WLAN frequencies through the incorporation of slits on each antenna [7]. Tripathi et al. [8] have implemented a compact octagonal UWB-MIMO antenna designed to minimize Wireless LAN narrowband interference by incorporating a C-shaped slot and enhancing isolation. A compact MIMO antenna using a band-rejection filter to enhance isolation has been investigated [9]. In [10], a MIMO antenna is characterized by high isolation, employing a stepped stub for decoupling, and being capable of rejecting signals within designated frequencies. In [11], a unique UWB-MIMO Vivaldi aerial characterized by enhanced element isolation and a singular rejection feature, is achieved through the integration of a T-type groove and two optimally positioned split ring resonators. A two-port compact UWB-MIMO aerial that can generate notches in two frequency bands with the incorporation of grooves and stub is investigated in [12]. In [13], a planar, compact, and low-cost printed microstrip line fed pentagon-shaped UWB antenna offering dual band notched characteristics is investigated. In [14–33], several compact UWB-MIMO aerials with improved separation with single, dual, and triple frequency rejection capabilities were developed. In [34, 35], quadruple band notched UWB MIMO antennas without any decoupling element is proposed.

To effectively minimize interference to a negligible level, it is crucial to suppress significant interference bands within the UWB spectrum. Current literature on UWB antenna designs

* Corresponding author: Sadineni Ramesh Babu (srameshbabu@rvrjc.ac.in).

mainly focuses on strategies for mitigating one or two band notches, with little attention given to techniques for rejecting triple bands. Additionally, the UWB antenna designs explored in the literature tend to be large and impractical for portable devices. This article proposes a MIMO antenna design with robust isolation, capable of suppressing three distinct frequency bands within the ultra-wideband spectrum. The proposed design ensures superior isolation of over -20 dB, which is critical for the performance of MIMO systems.

2. UNIT ANTENNA ELEMENT

Figure 1 demonstrates the optimum geometric configuration of the triple band rejection UWB antenna. The suggested antenna incorporates an optimized rectangular radiator made of copper, lithographed on an FR4 substrate. The aerial has overall dimensions of $20 \times 24 \times 1.6\,\text{mm}^3$, with the following optimal dimensions (mm): $L = 24$, $W = 20$, $L_p = 12$, $W_p = 12$, $W_g = 20$, $L_g = 8.5$, $W_f = 2.5$, $L_f = 10$, $L_1 = 8$, $L_2 = 7$, $L_3 = 6.2$, $W_1 = 8.5$, $W_2 = 7$, $W_3 = 5.5$, $a = 2$, $b = 2$, $c = 2$, $d = 3$, $R = 3.8$.

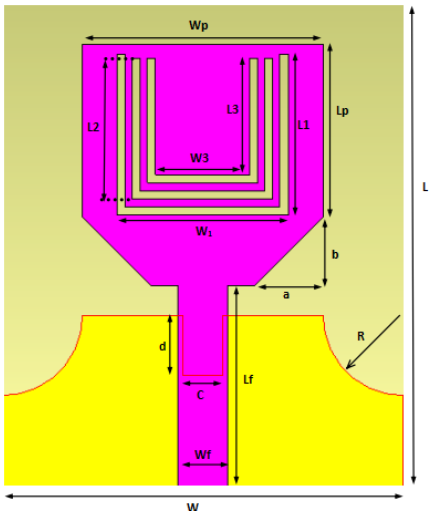

FIGURE 1. Suggested antenna geometry.

The reported aerial (shown in Figure 1) and its evolution is demonstrated in Figure 2. Firstly, a rectangular radiator is mounted on the substrate (Ant-1) as illustrated in Figure 2(a). This arrangement leads to an inconsistency in the feed connection, leading to current density at the antenna's bottom corners, hence diminishing radiation efficacy at elevated frequencies. To address this problem, Ant-2 is presented, incorporating two circular slots over the top corners of the ground and a central slot. Furthermore, the patch bottom edges are tapered to improve impedance bandwidth. To establish the band-notched features, the mentioned Ant-2 is equipped with a U-shaped slot (Slot #1), resulting in the formation of Ant #3 as illustrated in Figure 2(c). Consequently, Ant-3, with its configuration, can effectively reject a singular interfering band inside the 3.6–4.1 GHz range (downlink C-band). Therefore, to enhance the rejection capabilities, an additional open-ended U-slot (Slot #2) is introduced. Consequently, Ant-4 is acquired, which can eliminate two distinct interfering bands: 3.6–4.1 GHz and 4.43–4.79 GHz (INSAT). Additionally, another U-shaped slot (Slot #3) is included to create Ant-5. Thus, Ant-5 can suppress three interfering bands 3.6–4.1 GHz, 4.43–4.79 GHz, and 5.25–5.75 GHz (WLAN). Therefore, to ensure the presence of notches, the cumulative slot lengths can be readily computed by using following equations [36].

$$U_{slot\#1} = 2 \times (L_1) \times W_1 = \frac{c}{2f_n\sqrt{\varepsilon_{eff}}} \tag{1}$$

$$U_{slot\#2} = 2 \times (L_2) \times W_2 = \frac{c}{2f_n\sqrt{\varepsilon_{eff}}} \tag{2}$$

$$U_{slot\#3} = 2 \times (L_3) \times W_3 = \frac{c}{2f_n\sqrt{\varepsilon_{eff}}} \tag{3}$$

$$\varepsilon_{eff} = \frac{\varepsilon_r + 1}{2} \tag{4}$$

where C is the free space light velocity, and ε_{eff} is the effective dielectric constant of the substrate.

Variables L_1, L_2, L_3, W_1, W_2, and W_3 represent the lengths of the corresponding slots.

$|S_{11}|$ curves for Ant-1 through Ant-5 are illustrated in Figure 3. A rectangular antenna (Ant-1) is first developed to achieve an impedance spectrum of 5 GHz. The optimized Ant-2 operates across UWB spectrum, covering from 3 to 12 GHz. Ant-3, Ant-4, and Ant-5 are simulated separately for examining notch behavior. The three U-shaped slots generate notches at 3.9 GHz (downlink C-band), 4.6 GHz (INSAT), and 5.5 GHz (Wireless LAN) as illustrated in Figure 3.

2.1. Parametric Study

Parametric analyses for Ant-3, Ant-4, and Ant-5 regarding three slots are conducted to comprehend the impact of notched frequencies. Figure 4 illustrates the reflection coefficient characteristics, enabling a comparative analysis of the control exerted over the rejection process. L_1, L_2, L_3, W_1, W_2, and W_3 are the vital parameters for obtaining band notch behavior. The values are crucial because the currents traverse in opposite direction in slots at designated notch frequencies. To achieve optimal design, only one parameter is optimized sequentially. Reflection coefficient characteristics for the triple band rejected UWB aerial are displayed in Figures 4(a)–(c). The figure shows that as the slot length increases, the frequency range targeted for signal blocking shifts downward. On the flip side, a shorter slot length moves desired stopband upward. It is shown in Eqs. (1)–(3) that the intended signal blocking frequency has inverse relation to slot length. Also, the notch frequencies are shown to be fundamentally independent of one another. So, to get the necessary notch frequency and bandwidth, size and position adjustment is necessary for the components that govern the frequency band and notches.

2.2. Time Domain Analysis

The group delay metric accounts for the lag in transmission and reception, making it a crucial parameter for temporal domain research. By considering the negative sign derivative of the

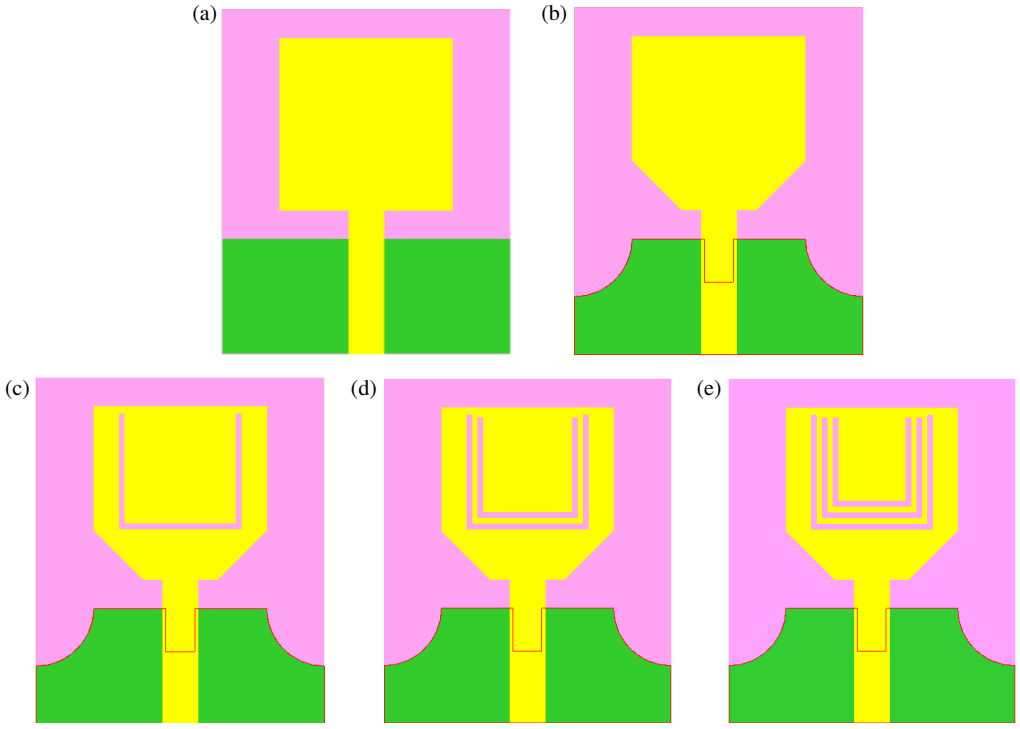

FIGURE 2. Unit antenna element evolution. (a) Ant-1. (b) Ant-2. (c) Ant-3. (d) Ant-4. (e) Ant-5.

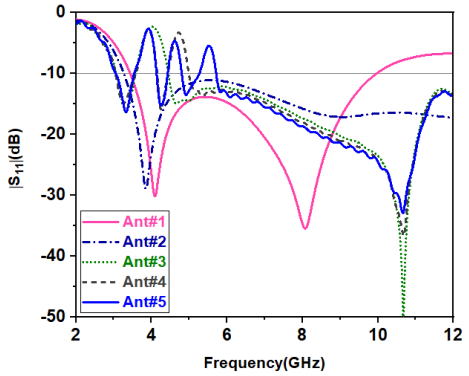

FIGURE 3. Simulated $|S_{11}|$.

changing phase and frequency, this delay may be analytically computed. As they travel through the measuring instruments, the transmitted signals acquire some undesired distortion. The identical measuring antenna pair is separated by a distance of 320 mm. Figure 5 illustrates the side-by-side and face-to-face arrangements considered for evaluating the wave signals in this study. As demonstrated in Figure 5, except at notch frequencies, the group delay curves in both scenarios range approximately between 1 and 2 nsec.

2.3. Equivalent Circuit Analysis

An equivalent circuit is constructed for the suggested triple band-suppressed UWB antenna, aimed at elucidating the mechanism behind band-notched structures. Figure 6(a) illustrates the impedance curve of the UWB aerial devoid of notch structures. The real impedance is around 50 Ω, while the imaginary component is around 0 Ω. This enhances impedance match in the impedance bandwidth. Figure 6(b) exhibits the impedance curve of UWB antenna with notches. At central notch frequencies of 3.9 GHz, 4.6 GHz, and 5.5 GHz, the real component of the impedance approximates 50 Ω, and the imaginary component's slope transitions from negative to positive, indicating series resonance characteristics.

The Advanced Design System software is utilized to model the RLC circuit, providing the corresponding circuit representation as demonstrated in Figure 6(c). Additionally, Figure 6(d) illustrates a comparative analysis of simulation outcomes obtained from the circuit model and those derived from CST simulations. The values of the RLC elements and quality factor Q_0 are calculated using Eqs. (5)–(7), as specified in Table 1 [36].

$$f_{notch,i} = \frac{1}{2\pi\sqrt{L_i C_i}} \tag{5}$$

TABLE 1. Calculated R, L, C values.

	BW (GHz)	Q_0	R in Ω	L in nH	C in pF
UWB antenna	3–12	-	50	0.147	10.2
First notch (3.9 GHZ)	0.6	6.5	10	2.65	0.628
Second notch (4.6 GHZ)	0.36	12.7	18	7.93	0.151
Third notch (5.5 GHZ)	0.46	11.9	50	0.017	0.0486

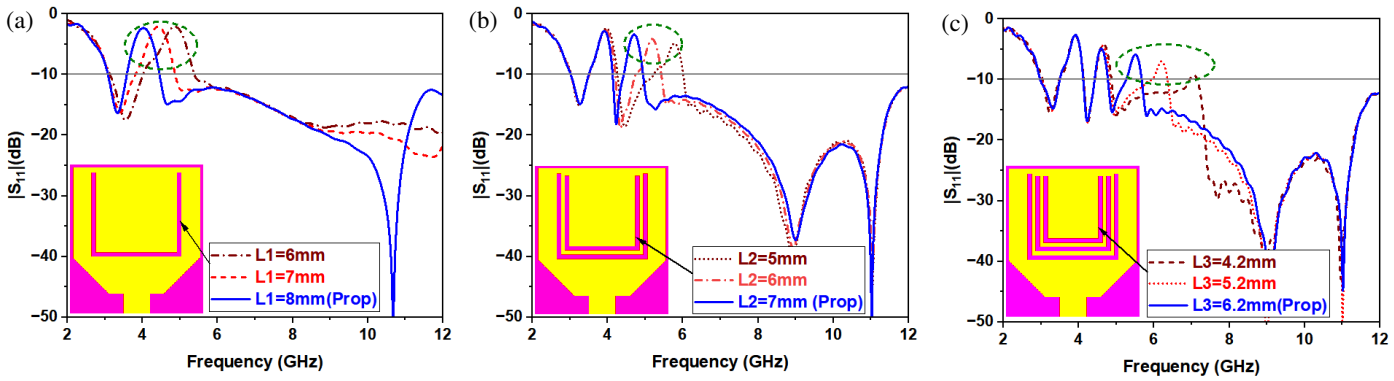

FIGURE 4. Reflection coefficient for variation in lengths of (a) slot #1, (b) slot #2, (c) slot #3.

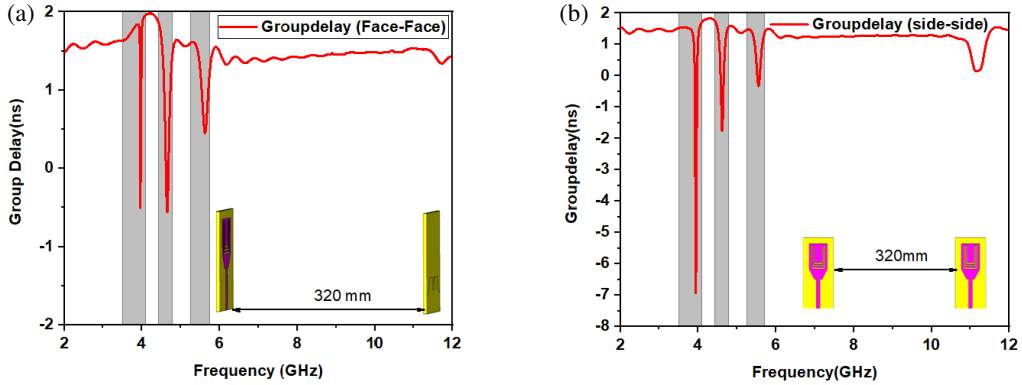

FIGURE 5. Group delay.

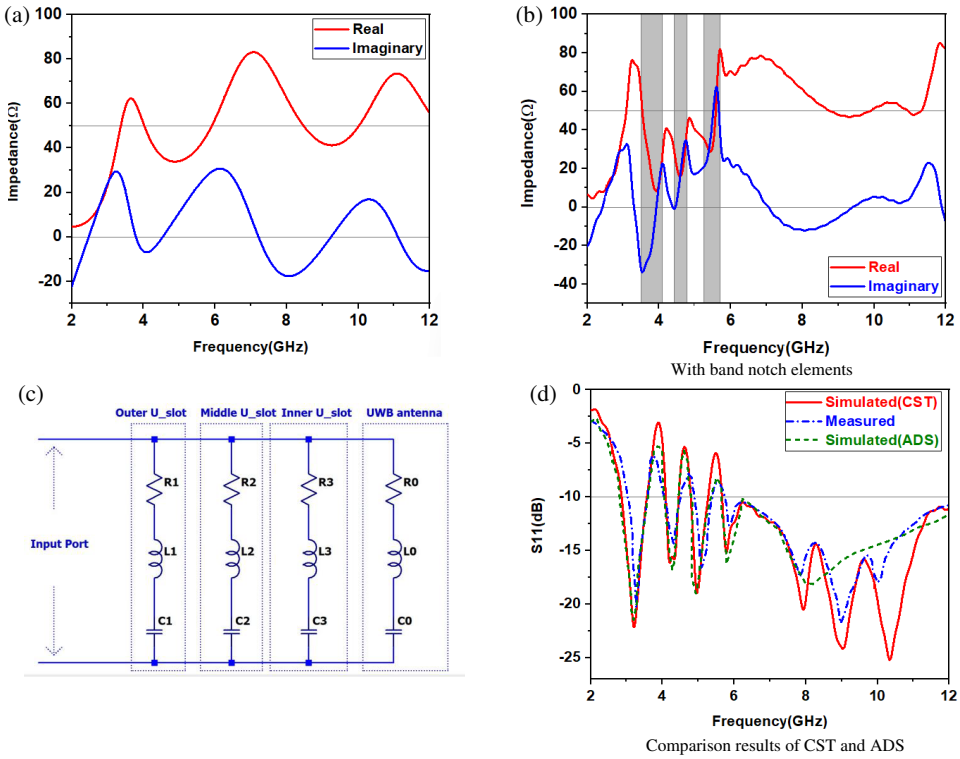

FIGURE 6. (a) Impedance curves without band notch elements. (b) Impedance curves with band notch elements. (c) Equivalent circuit. (d) $|S_{11}|$ curve.

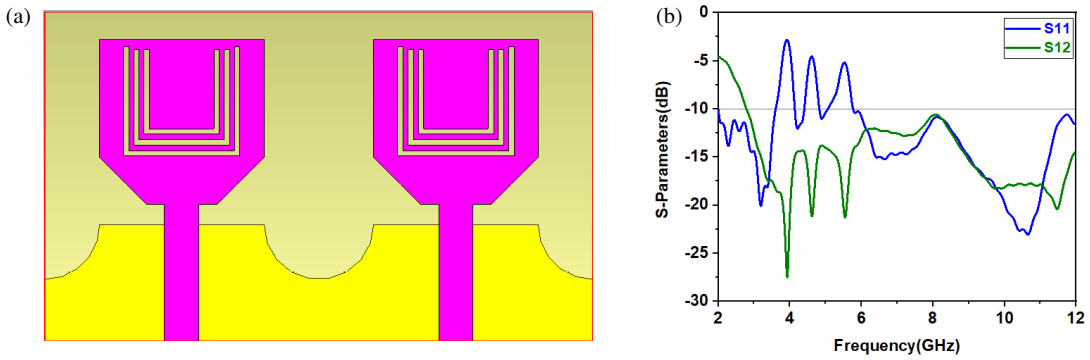

FIGURE 7. (a) Collinear antenna. (b) S-parameters.

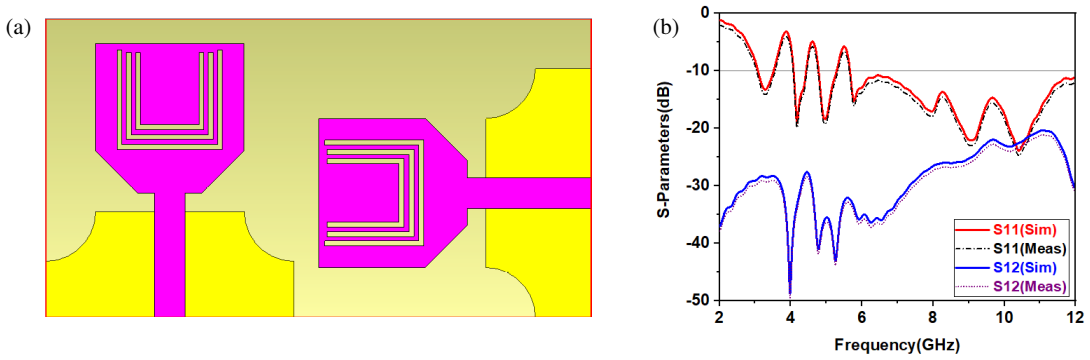

FIGURE 8. (a) Dual port orthogonal UWB-MIMO antenna. (b) S-parameters.

$$Q_0 = \frac{1}{2\pi f_{notch,i} R_i C_i} \tag{6}$$

$$BW = \frac{f_{notch,i}}{Q_0} \tag{7}$$

3. TWO ELEMENT MIMO CONFIGURATION

Figure 7 illustrates the layout of the UWB MIMO/diversity antenna with two ports. As depicted in Figure 7(a), the aerial embodies two identical radiators that are positioned in a collinear manner. Dimensions of the collinear antenna are 24 mm $\times$ 40 mm $\times$ 1.6 mm.

Simulated S-parameter results demonstrated in Figure 7(b) illustrate that three notches exist in the UWB. The inter element isolation is below -10 dB, which is insufficient for MIMO applications, in which isolation should be below -20 dB. Figure 8(a) shows that the antennas are oriented in orthogonal manner to enhance isolation utilizing polarization diversity. The S-parameter results demonstrate that the antenna attains three notches in UWB and inter-element isolation less than -20 dB as demonstrated in Figure 8(b).

Polarization diversity reduces mutual coupling better than collinear configuration and achieves an isolation of -20 dB. In MIMO systems, antenna element correlation and diversity gain are crucial metrics for characterizing diversity performance. Envelope correlation coefficient (ECC) (ρ) between nearby antennas and diversity gain are computed by

$$ECC = \frac{|S_{ii} * S_{ij} + S_{ji} * S_{jj}|^2}{\left(1 - |S_{ii}|^2 - S_{ij}^2\right)\left(1 - |S_{ji}|^2 - S_{jj}^2\right)} \tag{8}$$

$$DG = 10\sqrt{1 - ECC^2} \tag{9}$$

The calculated ECC for the suggested UWB MIMO aerial is < 0.05 and DG around 10 dB across the whole impedance bandwidth as depicted in Figure 9. The low ECC and 10 dB diversity gain values indicate that the reported MIMO antenna has the capability to deliver excellent diversity performance.

4. FOUR ELEMENT MIMO CONFIGURATION

Pertaining to the polarization diversity phenomena utilized by the dual-port UWB MIMO aerial, the neighbouring aerial elements are configured orthogonally, resulting in the development of a quad-port UWB MIMO antenna. The four-port UWB MIMO aerial layout without any decoupler on the ground plane and its S-parameters are illustrated in Figure 10.

The impedance frequency spectrum of the reported quad-port antenna spans from 3 to 12 GHz, featuring three notched bands: 3.6–4.1 GHz, 4.43–4.79 GHz, and 5.25–5.71 GHz, as illustrated in Figure 10. The inter-element isolation S_{12} and S_{14} are less than -20 dB due to polarization diversity. However, inter-element isolation between Antenna #1 and Antenna #3 (S_{13}) is around -17 dB only across the entire UWB frequency spectrum. Ideally, an isolation of -20 dB is required for a MIMO configuration. To enhance the inter-element isolation between Antenna #1 and Antenna #3 to below -20 dB across the full UWB range, additional modifications were implemented in the four-port antenna with 4 mm gap between adjacent antenna elements. A fan-shaped decoupler was integrated into the ground plane, as shown in Figures 11(a) and 11(b), significantly improving the isolation between the an-

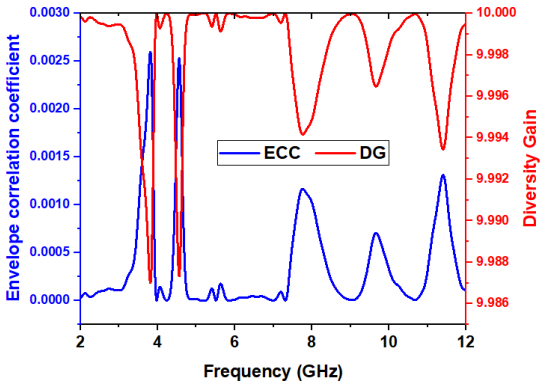

FIGURE 9. ECC and diversity gain.

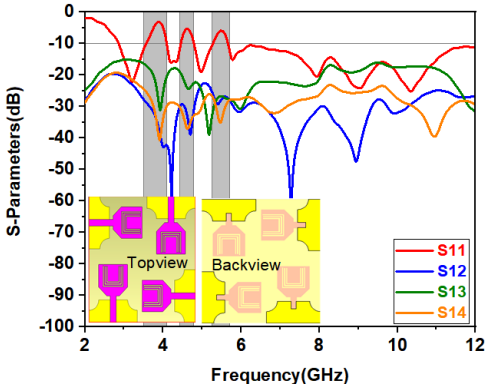

FIGURE 10. S-parameters (without decoupler).

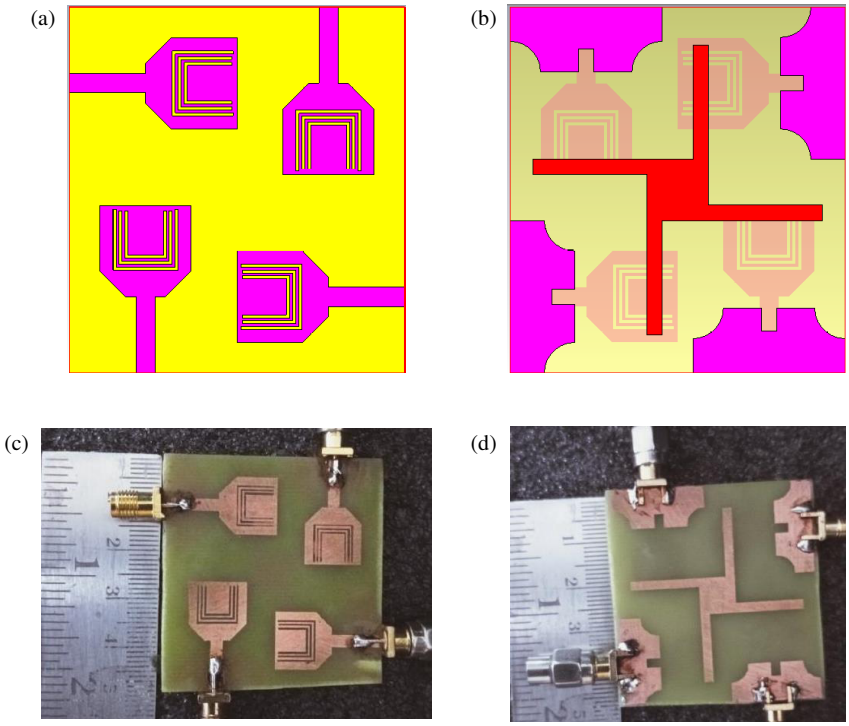

FIGURE 11. Configuration of four port UWB MIMO antenna with decoupler (Top view). (b) Bottom view. (c) Prototype top-view. (d) Prototype bottom view.

tenna ports. Figures 11(c) and 11(d) display the prototype model.

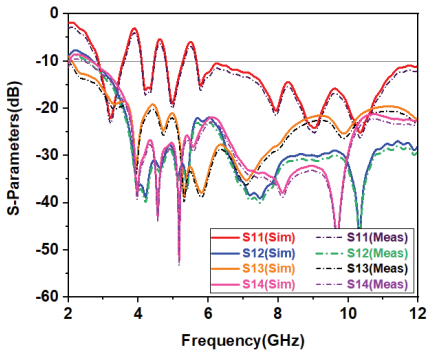

FIGURE 12. Simulated and measured s-parameters.

For design and simulation, CST MW Studio is utilized, while a vector network analyzer performs measurements to thoroughly evaluate the aerial performance. Due to antenna symmetry, the behavior of one antenna reflects that of the others. Therefore, only the S-parameters for Antenna #1 are presented here. Figure 12 illustrates the simulated and measured S-parameter outcomes of the UWB MIMO antenna.

5. RESULTS AND DISCUSSION

Figure 13 illustrates surface current variation of the suggested aerial at three notch frequencies. When port-1 is activated while the other ports are deactivated, the current density concentrates at outermost slot at 3.9 GHz, around the central slot at 4.6 GHz, and at the inner slot at 5.5 GHz. The band-notch configuration induces the current to traverse in the reverse direction along

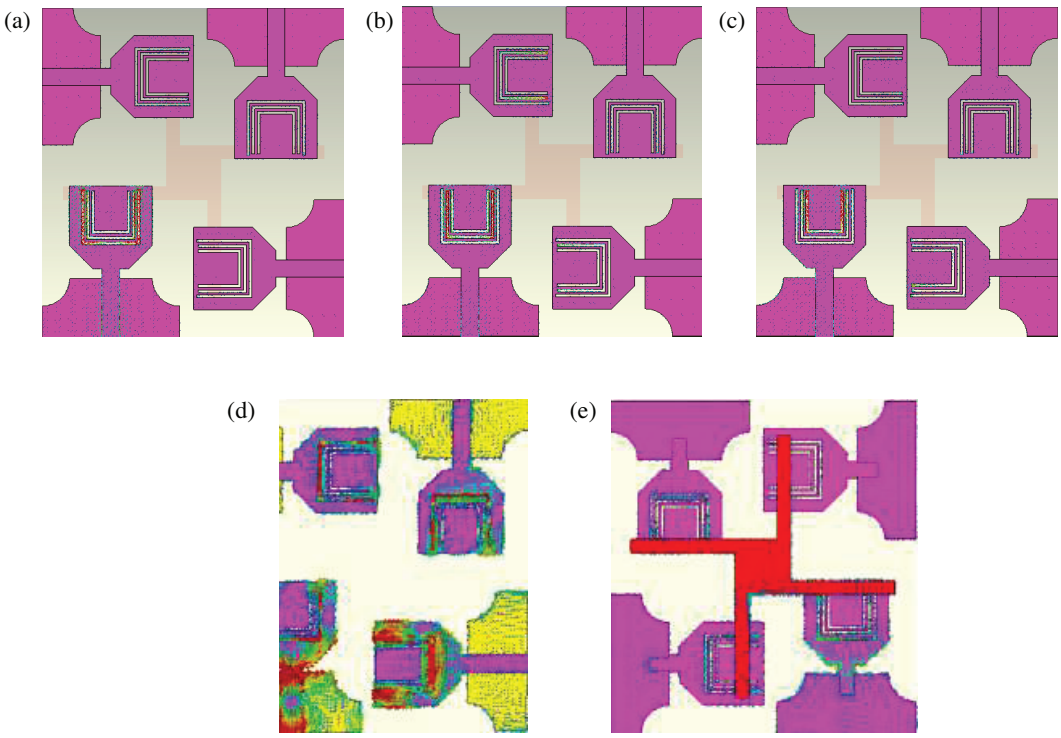

FIGURE 13. Surface current variation at (a) 3.9 GHz, (b) 4.6 GHz, (c) 5.5 GHz, (d) surface current distribution between Ant #1 and Ant #3 without decoupler (e) with decoupler.

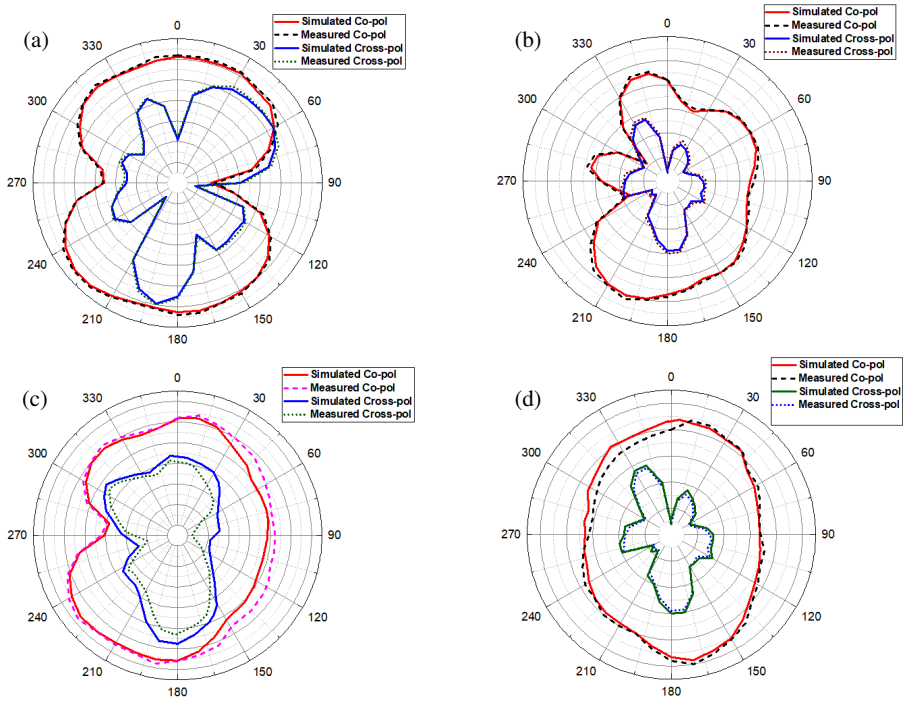

FIGURE 14. Normalized radiation characteristics at (a) 4.17 GHz (E-Plane), (b) 4.17 GHz (H-Plane), (c) 4.91 GHz (E-Plane), (d) 4.91 GHz (H-Plane).

the diverging edges, thus nullifying the radiation fields. Consequently, the aerial acts as a non-radiating structure at notch frequencies.

Figures 14(a)–14(d) illustrate the radiation characteristics at two resonant frequency points: 4.17 GHz and 4.91 GHz. Each plot includes co-pol and cross-pol patterns for E- and H-planes. Ant-1 port is excited, while the remaining ports are terminated

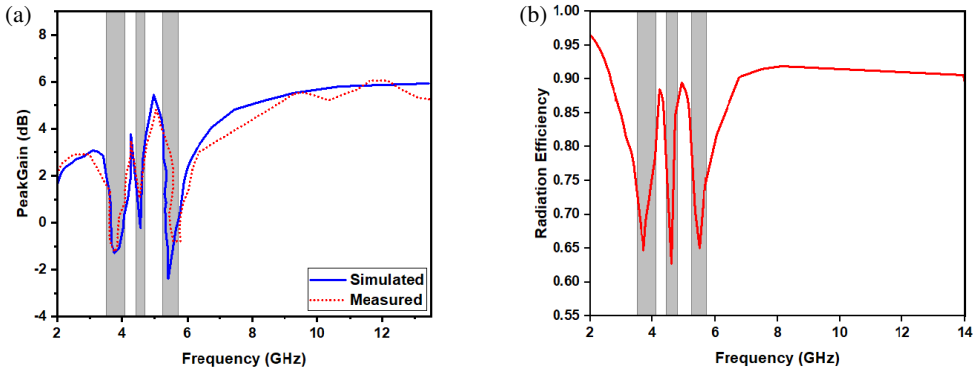

FIGURE 15. (a) Peak gain. (b) Radiation efficiency.

with 50 Ω load. Consequently, the patterns at designated frequencies are bidirectional in E-plane and omnidirectional in H-plane. As evidenced by Figure 14, co-pol results exceed cross-pol characteristics.

Figure 15(a) illustrates the peak gain of the aerial, which remains largely steady throughout operational bandwidth, with the exception for a dip at three notch frequencies, signifying effective attenuation of intrusion from downlink C-band, INSAT, and WLAN. The gain is the lowest in notch frequency bands of 3.6–4.1 GHz, 4.43–4.79 GHz, and 5.25–5.71 GHz. The simulated gain spans from 2 to 6 dBi, while the observed gain value varies between 2 and 5 dBi. The measured antenna's maximum gain is inferior to the modeling result because of flaws in physical processing and environmental interference during measurement. The aerial's radiation efficiency is around 90% across the whole UWB frequency spectrum, except at notches. The antenna's radiation efficiency in the triple notched frequency bands is below 65%.

5.1. Diversity Characteristics

MIMO antennas capabilities and performance could be verified using measurements of critical metrics such as ECC, DG, TARC, CCL, and multiplexing efficiency [36].

5.2. Envelope Correlation Coefficient

Envelope correlation coefficient (ECC) is used for interference assessment among array elements. Consequently, to guarantee dependable MIMO functionality, the appropriate results of ECC must be below 0.5. ECC could be derived from the far-field results, as stated in Eq. (10)

$$ECC = \frac{\left|\int_0^{2\pi}\int_0^{\pi}(XPRE_{\theta 1}E^*_{\theta 2}P_\theta + E_{\varphi 1}E^*_{\varphi 2}P_\varphi)d\Omega\right|^2}{\int_0^{2\pi}\int_0^{\pi}(XPRE_{\theta 1}E^*_{\theta 1}P_\theta + E_{\varphi 1}E^*_{\varphi 1}P_\varphi) d\Omega X (XPRE_{\theta 2}E^*_{\theta 2}P_\theta + E_{\varphi 2}E^*_{\varphi 2}P_\varphi)d\Omega} \quad (10)$$

5.3. Diversity Gain

Diversity gain (DG) quantifies the enhancement in signal-to-noise ratio (SNR) attained. ECC and diversity gain are interrelated, as illustrated in Eq. (11)

$$DG = 10\sqrt{1 - ECC^2} \quad (11)$$

Figures 16(a) and (b) show that ECC is < 0.16 and diversity gain (DG) is 9.98 dB across whole frequency spectrum, except at notches. This demonstrates the efficacy of reported UWB-MIMO aerial.

5.4. Total Active Reflection Coefficient

Total active reflection coefficient (TARC) is used to represent mutual and self-impedance of MIMO antennas. In practice, an acceptable TARC value is equal to or lower than 0 dB. To verify the effect of TARC on impedance bandwidth, the proposed four-port MIMO antenna is integrated with an ideal phase shifter where a scan angle is fixed at 180°. TARC may be assessed as

$$TARC = \frac{\sqrt{\sum_{i=1}^{4}\left|S_{i1} + \sum_{n=2}^{4} S_{in}e^{j\theta n-1}\right|^2}}{2} \quad (12)$$

5.5. Channel Capacity Loss

Channel capacity loss (CCL) serves to assess the maximum possible signal transmission rate. Predominantly, CCL is generally expected to be below 0.4 bits per second per Hertz. Figure 16(c) illustrates that CCL and TARC values were below 0.4 bps/Hz and −10 dB throughout the operational bandwidth except at notch frequencies. CCL is expressed as

$$CCL = -\log_2 \det\left|\psi^R\right|$$
$$\psi^R = \begin{bmatrix} \rho 11 & \rho 12 & \rho 13 & \rho 14 \\ \rho 21 & \rho 22 & \rho 23 & \rho 24 \\ \rho 31 & \rho 32 & \rho 33 & \rho 34 \\ \rho 41 & \rho 42 & \rho 43 & \rho 44 \end{bmatrix} \quad (13)$$

5.6. Multiplexing Efficiency

The multiplexing efficiency (η_{mux}) is calculated by the following Eq. (14).

$$\eta_{mux} = \sqrt{\eta_i \eta_j \left(1 - |\rho_c|^2\right)} \quad (14)$$

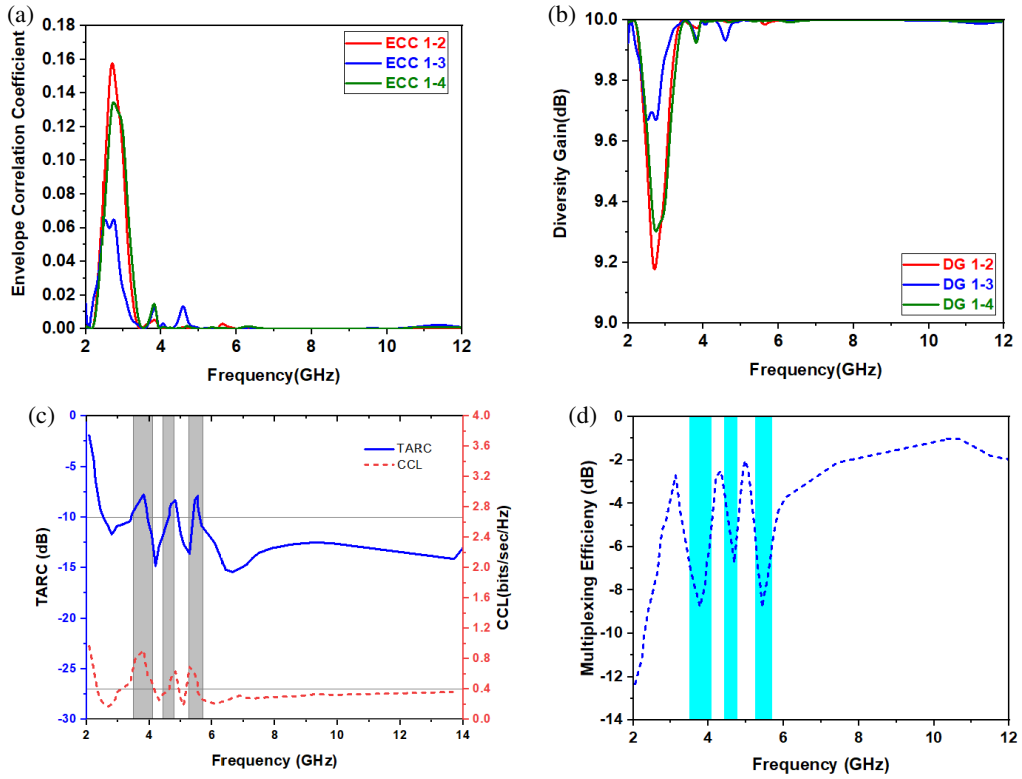

FIGURE 16. (a) ECC. (b) Diversity gain. (c) TARC and CCL. (d) Multiplexing efficiency.

TABLE 2. Comparison with existing designs.

Ref.	Size (mm^2)	BW	No. of notches	No. of Ports	Isolation (dB)	ECC
[8]	45×45	2–10.6	1	4	-17	< 0.01
[10]	30×30	3.1–11	1	2	-20	< 0.02
[12]	19×30	3.1–10.6	2	2	-18	< 0.13
[15]	64×45	2.5–11	3	2	-15	< 0.02
[22]	50×82	2.2–13.35	1	2	-15	< 0.04
[23]	18×36	2.2–20	1	2	-20	< 0.08
[24]	35×68	3.1–10.6	2	2	-20	< 0.002
[25]	30×22	3.1–10.6	1	2	-15	< 0.05
[26]	22×36	3.1–11	1	2	-15	< 0.1
[27]	41×41	2.95–10.65	2	2	-16	< 0.15
[28]	48×48	2.5–12	1	2	-15	< 0.005
[29]	44×44	2.95–10.8	1	4	-15.5	< 0.1
[30]	60×60	3–16.2	1	4	-17.5	< 0.4
[31]	100×100	2–15	2	4	-20	< 0.1
[32]	78×78	2.33–16	3	4	-20	< 0.05
[33]	40×21	2.94–11.61	1	2	-18	< 0.002
Proposed	**44×48**	**3–12**	**3**	**4**	**-2**	**<0.16**

Figure 16(d) indicates that the multiplexing efficiency exhibits triple-band notch features. Throughout the whole impedance bandwidth (3–12 GHz), excluding notch frequencies, the multiplexing efficiency exceeds -3 dB, indicating that the UWB-MIMO antenna possesses exceptional multiplexing efficiency.

5.7. Group Delay

Group delay is a temporal feature of MIMO antennas. Figure 17 illustrates the fluctuations in group delay of 4 antenna elements across the UWB spectrum. Group delay (1-1) represents port 1 to port 1 delay, while group delays (1-2), (1-3), and (1-4) corre-

spond to the delays from port 1 to port 2, 3, and 4, respectively. Due to the same and symmetrical nature of the elements in the suggested MIMO antenna, group delays from 1 to 2 and 4 exhibit nearly identical characteristics, as illustrated in Figure 17. The recommended MIMO antenna has group delays < 1.5 ns, except at notch frequencies. Figure 18 shows the proposed antenna measurement inside an anechoic chamber.

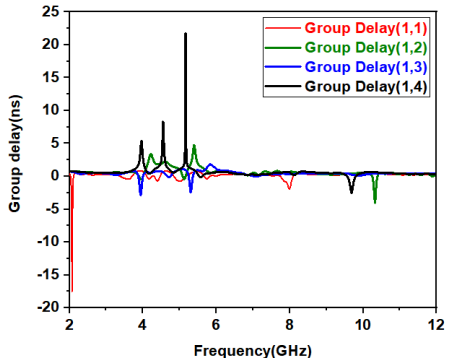

FIGURE 17. Group delays.

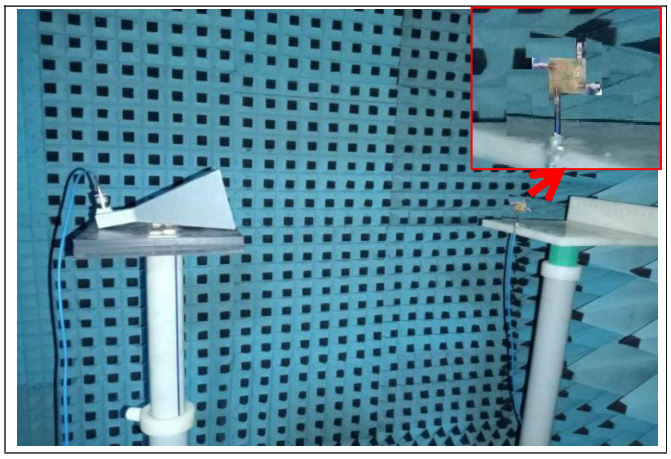

FIGURE 18. Measurement inside anechoic chamber.

Additionally, the suggested antenna efficacy was assessed by juxtaposing it with the results of prior studies, and the outcomes are encapsulated in Table 2. A thorough examination of the efficacy of each antenna demonstrated in the table reveals that the antenna attains a broader operational frequency spectrum and enhanced isolation while maintaining structural miniaturization.

6. CONCLUSION

This study presents a miniaturized UWB-MIMO aerial with triple band suppression characteristics measuring $44 \times 48 \times 1.6\,\text{mm}^3$. Inter-element isolation among antenna structures is diminished by utilizing a fan-shaped decoupler on the ground, while the notch frequency bands are generated through the introduction of three U-shaped slots. Measured results indicate that the fabricated antenna demonstrates $|S_{11}| < -10$ dB, enhanced isolation exceeding 20 dB, peak gain ranging from 2 dBi to 6 dBi, radiation efficiency fluctuating between 65% and 90%, ECC < 0.16, and TARC < -10 dB across the ultra wideband, with the exception of three notched bands at 3.6–4.1 GHz, 4.43–4.79 GHz, and 5.25–5.71 GHz. All measured and simulated outcomes demonstrate that the suggested quad-port MIMO antenna is a suitable choice for UWB applications.

REFERENCES

[1] Federal Communications Commission, "Revision of part 15 of the commission's rules regarding ultra-wideband transmission system from 3.1 to 10.6 GHz," 98–153, 2002.

[2] Liu, L., S. W. Cheung, and T. I. Yuk, "Compact MIMO antenna for portable devices in UWB applications," *IEEE Transactions on Antennas and Propagation*, Vol. 61, No. 8, 4257–4264, 2013.

[3] Li, Z., C. Yin, and X. Zhu, "Compact UWB MIMO Vivaldi antenna with dual band-notched characteristics," *IEEE Access*, Vol. 7, 38 696–38 701, 2019.

[4] Zhang, S. and G. F. Pedersen, "Mutual coupling reduction for UWB MIMO antennas with a wideband neutralization line," *IEEE Antennas and Wireless Propagation Letters*, Vol. 15, 166–169, 2015.

[5] Wang, H., D. G. Fang, and X. L. Wang, "Mutual coupling reduction between two microstrip patch antennas by using the parasitic elements," in *2008 Asia-Pacific Microwave Conference*, 1–4, Hong Kong, China, 2008.

[6] Acharjee, J., K. Mandal, and S. K. Mandal, "Reduction of mutual coupling and cross-polarization of a MIMO/diversity antenna using a string of H-shaped DGS," *AEU — International Journal of Electronics and Communications*, Vol. 97, 110–119, 2018.

[7] Zhu, J., S. Li, B. Feng, L. Deng, and S. Yin, "Compact dual-polarized UWB quasi-self-complementary MIMO/diversity antenna with band-rejection capability," *IEEE Antennas and Wireless Propagation Letters*, Vol. 15, 905–908, 2015.

[8] Tripathi, S., A. Mohan, and S. Yadav, "A compact Koch fractal UWB MIMO antenna with WLAN band-rejection," *IEEE Antennas and Wireless Propagation Letters*, Vol. 14, 1565–1568, 2015.

[9] Khan, M. S., A. D. Capobianco, S. Asif, A. Iftikhar, B. Ijaz, and B. D. Braaten, "Compact 4 × 4 UWB-MIMO antenna with WLAN band rejected operation," *Electronics Letters*, Vol. 51, No. 14, 1048–1050, 2015.

[10] Biswal, S. P. and S. Das, "A low-profile dual port UWB-MIMO/diversity antenna with band rejection ability," *International Journal of RF and Microwave Computer-Aided Engineering*, Vol. 28, No. 1, e21159, 2017.

[11] Li, Z., C. Yin, and X. Zhu, "Compact UWB MIMO Vivaldi antenna with dual band-notched characteristics," *IEEE Access*, Vol. 7, 38 696–38 701, 2019.

[12] Kumar, A., A. Q. Ansari, B. K. Kanaujia, J. Kishor, and S. Kumar, "An ultra-compact two-port UWB-MIMO antenna with dual band-notched characteristics," *AEU — International Journal of Electronics and Communications*, Vol. 114, 152997, 2020.

[13] Kadam, A. A. and A. A. Deshmukh, "Pentagonal shaped UWB antenna loaded with slot and EBG structure for dual band notched response," *Progress In Electromagnetics Research M*, Vol. 95, 165–176, 2020.

[14] Tang, Z., X. Wu, J. Zhan, S. Hu, Z. Xi, and Y. Liu, "Compact UWB-MIMO antenna with high isolation and triple band-notched characteristics," *IEEE Access*, Vol. 7, 19 856–19 865, 2019.

[15] Jaglan, N., S. D. Gupta, E. Thakur, D. Kumar, B. K. Kanaujia, and S. Srivastava, "Triple band notched mushroom and unipla-

nar EBG structures based UWB MIMO/Diversity antenna with enhanced wide band isolation," *AEU — International Journal of Electronics and Communications*, Vol. 90, 36–44, 2018.

[16] Doddipalli, S. and A. Kothari, "Compact UWB antenna with integrated triple notch bands for WBAN applications," *IEEE Access*, Vol. 7, 183–190, 2018.

[17] Chen, Z., W. Zhou, and J. Hong, "A miniaturized MIMO antenna with triple band-notched characteristics for UWB applications," *IEEE Access*, Vol. 9, 63 646–63 655, 2021.

[18] Kumar, P., S. Urooj, and F. Alrowais, "Design of quad-port MIMO/Diversity antenna with triple-band elimination characteristics for super-wideband applications," *Sensors*, Vol. 20, No. 3, 624, 2020.

[19] Sadineni, R. B. and D. P. Gowda, "Design of penta-band notched UWB MIMO antenna for diverse wireless applications," *Progress In Electromagnetics Research M*, Vol. 107, 35–49, 2022.

[20] Kumar, P., T. Ali, and M. P. Mm, "Characteristic mode analysis-based compact dual band-notched UWB MIMO antenna loaded with neutralization line," *Micromachines*, Vol. 13, No. 10, 1599, 2022.

[21] Mukherjee, S., A. Roy, S. Maity, T. Tewary, P. P. Sarkar, and S. Bhunia, "Design of dual band-notched UWB hexagonal printed microstrip antenna," *International Journal of Microwave and Wireless Technologies*, Vol. 15, No. 3, 526–534, 2023.

[22] Toktas, A., "G-shaped band-notched ultra-wideband MIMO antenna system for mobile terminals," *IET Microwaves, Antennas & Propagation*, Vol. 11, No. 5, 718–725, 2017.

[23] Chandel, R. and A. K. Gautam, "Compact MIMO/diversity slot antenna for UWB applications with band-notched characteristic," *Electronics Letters*, Vol. 52, No. 5, 336–338, 2016.

[24] Li, W. T., Y. Q. Hei, H. Subbaraman, X. W. Shi, and R. T. Chen, "Novel printed filtenna with dual notches and good out-of-band characteristics for UWB-MIMO applications," *IEEE Microwave and Wireless Components Letters*, Vol. 26, No. 10, 765–767, 2016.

[25] Tao, J. and Q. Feng, "Compact UWB band-notch MIMO antenna with embedded antenna element for improved band notch filtering," *Progress In Electromagnetics Research C*, Vol. 67, 117–125, 2016.

[26] Liu, L., S. W. Cheung, and T. I. Yuk, "Compact MIMO antenna for portable UWB applications with band-notched characteristic," *IEEE Transactions on Antennas and Propagation*, Vol. 63, No. 5, 1917–1924, 2015.

[27] Srivastava, G. and B. K. Kanuijia, "Compact dual band-notched UWB MIMO antenna with shared radiator," *Microwave and Optical Technology Letters*, Vol. 57, No. 12, 2886–2891, 2015.

[28] Gao, P., S. He, X. Wei, Z. Xu, N. Wang, and Y. Zheng, "Compact printed UWB diversity slot antenna with 5.5-GHz band-notched characteristics," *IEEE Antennas and Wireless Propagation Letters*, Vol. 13, 376–379, 2014.

[29] Liu, Y.-Y. and Z.-H. Tu, "Compact differential band-notched stepped-slot UWB-MIMO antenna with common-mode suppression," *IEEE Antennas and Wireless Propagation Letters*, Vol. 16, 593–596, 2016.

[30] Wu, W., B. Yuan, and A. Wu, "A quad-element UWB-MIMO antenna with band-notch and reduced mutual coupling based on EBG structures," *International Journal of Antennas and Propagation*, Vol. 2018, No. 1, 8490740, 2018.

[31] Shehata, M., M. S. Said, and H. Mostafa, "Dual notched band quad-element MIMO antenna with multitone interference suppression for IR-UWB wireless applications," *IEEE Transactions on Antennas and Propagation*, Vol. 66, No. 11, 5737–5746, 2018.

[32] El-Gendy, M. S., M. M. M. Ali, E. B. Thompson, and I. Ashraf, "Triple-band notched ultra-wideband microstrip MIMO antenna with bluetooth band," *Sensors*, Vol. 23, No. 9, 4475, 2023.

[33] Devana, V. N. K. R., A. Beno, C. P. Devadoss, Y. Sukanya, C. V. R. Sankar, P. Balamuralikrishna, S. Chandrasekhar, and K. V. Babu, "A compact self isolated MIMO UWB antenna with band notched characteristics," *IETE Journal of Research*, Vol. 70, No. 8, 6677–6688, 2024.

[34] Sadineni, R. B. and P. Dinesha, "A compact highly isolated UWB-MIMO diversity antenna with quad band notch characteristics," in *2022 IEEE International Symposium on Smart Electronic Systems (iSES)*, 331–336, Warangal, India, 2022.

[35] Sadineni, R. B. and P. Dinesha, "Design and development of a miniaturized highly isolated UWB-MIMO diversity antenna with quad band notch characteristics," *Progress In Electromagnetics Research C*, Vol. 131, 197–208, 2023.

[36] Sadineni, R. B. and D. P. Gowda, "Design and development of sextuple band reject UWB-MIMO antenna for wireless applications," *Progress In Electromagnetics Research C*, Vol. 128, 231–246, 2023.